Sensors and Actuators B 239 (2017) 578–585

Contents lists available at ScienceDirect

Sensors and Actuators B: Chemical

journal homepage: www.elsevier.com/locate/snb

Ultra-sensitive benzene detection by a novel approach: Core-shell nanowires combined with the Pd-functionalization

Jae-Hun Kim [a], Hyoun Woo Kim [b,c,*], Sang Sub Kim [a,*]

[a] Department of Materials Science and Engineering, Inha University, Incheon 402-751, Republic of Korea, Republic of Korea
[b] Division of Materials Science and Engineering, Hanyang University, Seoul 133-791, Republic of Korea, Republic of Korea
[c] The Research Institute of Industrial Science, Hanyang University, Seoul 133-791, Republic of Korea

ARTICLE INFO

Article history:
Received 30 April 2016
Received in revised form 19 July 2016
Accepted 11 August 2016

Keywords:
SnO_2-ZnO
Core-shell nanowire
Pd-Functionalization
Benzene (C_6H_6)
Gas sensor

ABSTRACT

We have realized an excellent selective sensing to benzene (C_6H_6) by means of using SnO_2-ZnO core-shell nanowires functionalized with Pd nanoparticles. We obtained a response of 71 for 100 ppb of C_6H_6, which is the highest response reported thus far. The synergistic effects of variation of SnO_2/ZnO potential barriers and chemical sensitization of Pd are responsible for the highest C_6H_6-sensing performance. These results highlight the potential for using Pd functionalized nanowires as a sensing platform in detecting trace concentrations of benzene, which is applicable in the future sensor, including the disease diagnosis and the environmental monitoring.

1. Introduction

Benzene (C_6H_6) is a poisonous volatile organic compound, which can be emitted from daily-life things, construction materials, and various chemical processes [1,2]. Since C_6H_6 is extremely detrimental to human health [3,4], the detection of C_6H_6 accurately in very low concentration is of great importance. In addition, an emerging application of chemoresistive-type sensors is diagnosing diseases via detecting a particular biomarker, which has a strong correlation with a specific disease. It has been known that C_6H_6 is a recognized biomarker for leukemia [5,6]. To ensure the reliability of this application, biomarkers must be detected at ppb-level concentrations.

The advantages of chemoresistive-type sensors based on semiconducting metal oxides over other types of chemical sensors, include simplicity in operation, flexibility in mass production, potential for miniaturization and low cost [7–11]. Therefore, they have long been applied in practical sensor devices in a wide range of areas, such as environmental emission monitoring, health care, homeland security, and artificial olfaction [12–16].

Despite the recent advances regarding improvements in the sensitivity of chemoresistive-type sensors [17–21], ppb-scale detection still remains a challenge. Recently, multiply-networked semiconducting oxide nanowires (NWs) have been recognized as a reliable sensing platform for the detection of gaseous chemical species [22–24]. The use of the core-shell (C-S) structure is particularly effective in the detection of reducing gases when the shell has thickness similar to the Debye length of the shell material [25]. Earlier studies have reported the fabrication and sensing properties of networked SnO_2 [22], CuO [23], and ZnO [24] NWs grown on a deliberately-designed catalytic pad layer using a vapor-phase growth technique. The improved reducing gas-sensing performance of the C-S NWs was attributed to the enhanced radial modulation of the electron-depleted region in the shell layer.

In this study, we realized sensor materials with exceptional C_6H_6-sensing properties, in which a ppb-scale C_6H_6 detection was achieved using the hybrid structure of the SnO_2-ZnO C-S NWs functionalized with Pd nanoparticles (NPs), demonstrating their use as a sensor platform for the detection of trace levels of C_6H_6. We expect that Pd NPs will act as a promoter for C_6H_6 gas to interact with the C-S NWs, in addition to the possible resistance due to the presence of heterointerfaces.

* Corresponding authors.
E-mail addresses: hyounwoo@hanyang.ac.kr (H.W. Kim), sangsub@inha.ac.kr (S.S. Kim).

http://dx.doi.org/10.1016/j.snb.2016.08.071
0925-4005/

2. Experimental

2.1. Growth of networked SnO_2-ZnO C-S NWs

The following processes were used for the growth of the networked SnO_2-ZnO C-S NWs (Fig. S1). First, SnO_2 NWs were grown in a network on a catalytic Au pad layer using the vapor-growth method by evaporating a source of Sn. To form the networked NWs, a patterned interdigital electrode (IDE) was prepared using a conventional photolithographic process on a SiO_2 layer (200-nm-thick) grown on Si (100) substrates. The IDE consisted of Au (3-nm-thick), Pt (200-nm-thick) and Ti (50-nm-thick) layers from the top. The trilayer was deposited sequentially by sputtering. The Au pad layer played the role of a catalyst for the selective growth of SnO_2 NWs, the Pt layer was an electrical circuit, and the Ti layer was used to enhance the adhesion between the Pt layer and the substrate. The growth of the core NWs of SnO_2 was carried out in a horizontal quartz tube furnace at 900 °C for 15 min with N_2 and O_2 gases at flow rates of 300 and 10 sccm, respectively. With the IDE, SnO_2 NWs were grown, forming the networked junctions between the electrode digits. The detailed experimental procedure for the fabrication of networked SnO_2 NWs is described in an earlier report [22].

Second, the networked SnO_2 NWs were coated with ZnO shells by atomic layer deposition (ALD). This deposition technique is particularly effective for depositing a uniform, conformal layer on an irregularly shaped object. Diethylzinc ($Zn(C_2H_5)_2$, DEZn) and H_2O were used as precursors for the ALD process, in which the temperature and pressure of the reactor were set to 150 °C and 0.3 Torr, respectively. One cycle of the ALD process constituted the following ALD process; a DEZn dose time of 0.12 s, a 3 s purge with N_2, an H_2O dose time of 0.15 s, and a 3 s purge with N_2. The thickness of the ZnO shells could be controlled on the nanometer scale by changing the number of ALD cycles. In this study, the thickness of ZnO shells was adjusted to 80 nm, which was selected according to earlier results regarding SnO_2-ZnO C-S NWs [25]. The experimental procedure for the ALD process is described in more detail elsewhere [26–28]. For comparison, networked ZnO NWs were grown and fabricated as sensors. The preparation procedure of the ZnO NW sensors, which is described in detail in an earlier report [29], was similar to that used for the networked SnO_2 NW sensors.

2.2. Functionalization of pristine NWs and C-S NWs with Pd NPs

The Pd NPs were synthesized and attached to the pristine SnO_2 NWs, pristine ZnO NWs and SnO_2-ZnO C-S NWs by using the γ-ray radiolysis technique. The precursor solution consisted of 0.051 mM palladium chloride ($PdCl_2$, Kojima Chemicals Co.) dissolved in a mixed solvent of acetone (50 vol.%) and 2-propanol (50 vol.%). The NW samples were immersed in the precursor solution and then exposed to ^{60}Co γ-rays at the Korea Atomic Energy Research Institute (KAERI). For theγγ-ray exposure, the exposure time and an illumination intensity were set to 3 h and 10 kGy h^{-1}, respectively. The experimental procedure for the γ-ray radiolysis technique is described in detail in an earlier report [30].

2.3. Sensing measurement and materials characterization

The C_6H_6-sensing characteristics of the Pd NP-functionalized C-S NWs were investigated using a gas-sensing measurement system at 300 °C; this temperature was optimized during preliminary experiments (Fig. S2). Their selective sensing properties were evaluated with various reducing gases, such as carbon monoxide (CO), carbon dioxide (CO_2) and C_7H_8. The experimental procedure for the sensing measurements is described in detail in our earlier reports [31,32]. The sensor response for the gases tested in this study was evaluated using the relationship R_a/R_g, where R_a and R_g are the resistances in the absence and presence of an analyte gas, respectively. The microstructure and phase of the synthesized NW samples were examined by field-emission scanning electron microscopy (FE-SEM) and X-ray diffraction (XRD), respectively.

3. Results and discussion

First, the microstructure of the C-S NWs was examined. Fig. 1a shows a plain-view image of the resulting Pd NP-functionalized SnO_2-ZnO C-S NWs, revealing a highly networked volume of SnO_2-ZnO C-S NWs, which was achieved by using the deliberately designed IDE. The image reveals the entanglement of the C-S NWs, which can aid in chemiresistive electrical transport. Fig. 1b presents a representative FE-SEM image taken from an individual C-S NW functionalized with Pd NPs. It was observed that Pd NPs with a diameter of approximately 15 nm were uniformly distributed over the surface of the ALD-created ZnO shell. This confirms that γ-ray radiolysis is an effective technique for creating Pd NPs on metal oxide NWs. For comparison, a typical microstructure of the SnO_2 NWs functionalized with Pd NPs is shown in Fig. 1c. A schematic diagram of the sensor structure based on the C-S NWs with Pd NPs functionalized is illustrated in Fig. 1d. With this procedure, various combinations of C-S NWs can be realized and various kinds of metal NPs can be functionalized by changing the radiolysis solution.

X-ray diffraction was used to identify the phases of the Pd NP-functionalized SnO_2-ZnO C-S NWs. Fig. 1e shows typical XRD patterns of the samples; the upper and the lower XRD patterns were taken from pure SnO_2 NWs and SnO_2-ZnO C-S NWs, respectively, which were both functionalized with Pd NPs. The lower XRD pattern, recorded with Cu-Kα (1.5418 Å) radiation, showed that the Pd NP-functionalized SnO_2-ZnO C-S NWs were composed of SnO_2, ZnO and Pd phases. The SnO_2 tetragonal rutile phase has lattice parameters of a = 4.73 Å and c = 3.18 Å (JCPDS Card No. 88-0287), whereas the wurtzite phase of ZnO has lattice parameters of a = 3.24 Å and c = 5.205 Å (JCPDS Card No. 89-0511). This XRD pattern is evidence of the successful phase formation of Pd NP-functionalized SnO_2-ZnO C-S NWs.

The dynamic resistance curves of the Pd NP-functionalized SnO_2-ZnO C-S NWs for C_6H_6 were measured, as shown in Supplementary information (Fig. 2). The results obtained from the sensors fabricated from pristine SnO_2 NWs, pristine ZnO NWs, SnO_2 NWs functionalized with Pd NPs, and pure SnO_2-ZnO C-S NWs were included for comparison. All sensors tracked the changing C_6H_6 concentration in the environment. The resistance of the sensors decreased as C_6H_6 was supplied and was restored once the C_6H_6 flow was stopped and air was introduced. This type of resistance behavior can be explained based on a well-known *n*-type semiconductor sensing mechanism, which is outlined as follows. In ambient air, oxygen species that are adsorbed onto the surface of the NWs capture electrons in the conduction band of the NWs. This creates a local, electron-depleted region beneath the surface of the NWs, which radially suppresses the charge-carrier conduction channel along the NWs' length. When C_6H_6 gas molecules are supplied, they interact with the adsorbed oxygen species, forming volatile compounds that will desorb from the surface of the NWs. This will release the captured electrons back into the conduction band, leading to a thinning of the electron-depletion region and thereby a corresponding decrease in resistance. This is the source of the resistance variation observed in the NW samples tested in this study. In Fig. 2, the sensor responses were strongly dependent on the type of sensors, and the Pd functionalization greatly improved the C_6H_6-sensing response of the pure C-S NWs.

Fig. 3 summarizes the responses of the sensors to 100 ppb C_6H_6 to show the difference between the C_6H_6 responses with respect

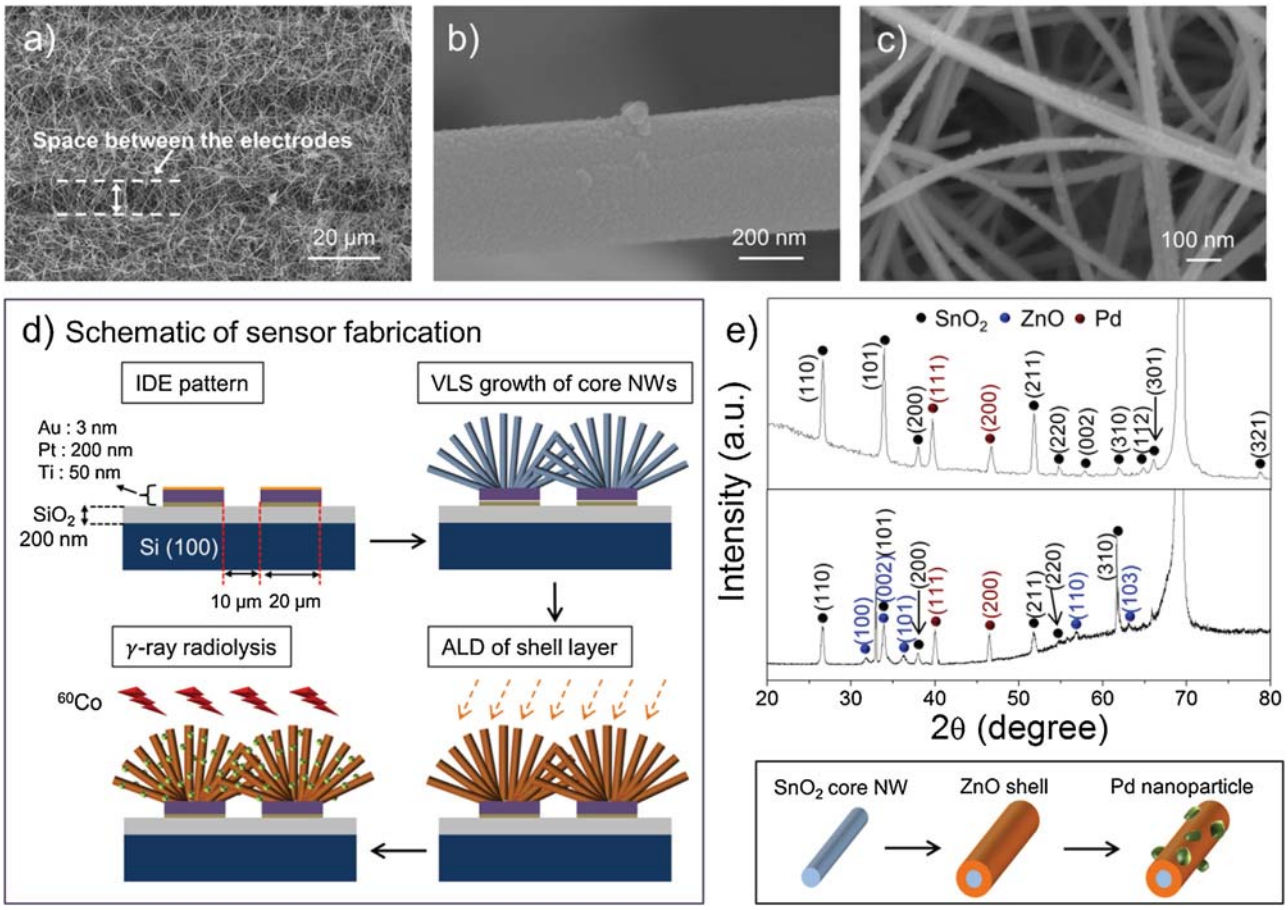

Fig. 1. Typical FE-SEM images; (a) Pd NPs-functionalized SnO_2-ZnO C-S NWs, (b) a single one, and (c) core SnO_2 NWs with Pd NPs functionalized. (d) Schematic of the sensor configuration used in this work. (e) Representative XRD patterns; the upper is for SnO_2 NWs with Pd NPs functionalized and the lower is SnO_2-ZnO C-S NWs with Pd NPs functionalized.

Table 1
Comparison of the C_6H_6-sensing response of the Pd NPs-functionalized SnO_2-ZnO C-S NWs in this work to those reported in the literatures.

Material type	C_6H_6 concentration (ppm)	Response (R_a/R_g)	Temp. (°C)	Reference
Porous SnO_2 microcubes	100	7	280	[33]
Partially broken WO_3 nanotubes	300	4	340	[34]
Pd-loaded SnO_2 yolk-shell nanostructures	5	6	450	[35]
Au/Porous ZnO microsheets	20	1.7	240	[36]
Au-ZnO NWs	10	4	340	[3]
Zn-W-O nanocomposite ceramic	100	4.1	370	[1]
TiO_2 thin films	10	1.00	RT	[2]
Ce-doped ZnO thin film	100	3.4	370	[37]
Titanium dioxide films dispersed in poly(vinylidenfluoride)	350	1.1	RT	[38]
Pd-functionalized SnO_2-ZnO C-S NWs (shell thickness 80 nm)	0.1	71	300	This work

to the type of NWs. The sensing temperature was set to 300 °C for a variety of sensors, with the preliminary understanding that the maximum sensing responses have been observed for those sensors in the present work (Text S1 in Supplementary information). The responses of pristine SnO_2 and pristine ZnO NWs to 1 ppm of C_6H_6 were 1.85 and 2.08, respectively, because they did not show any meaningful resistance variation for 100 ppb C_6H_6. By creating the ZnO shell layer on the pristine SnO_2 NWs, the C_6H_6 response increased greatly up to 11.2. The Pd functionalization on the SnO_2 NWs also improved the sensing response up to 30 for 100 ppb C_6H_6, which highlights the favorable role of Pd in the detection of C_6H_6 gas molecules. With the SnO_2-ZnO C-S NWs functionalized with Pd NPs, a response of 71.0 was obtained for 100 ppb C_6H_6. Taking both the C_6H_6 concentration and corresponding response into account, this is the highest C_6H_6 response reported so far in the literature (Table 1) [1–3,33–38], and it is sufficient for use in exhaled breath sensors that usually require ppb-scale detection. The C_6H_6 response of the Pd NP-functionalized SnO_2-ZnO C-S NWs was compared with those reported in the literature in Table 1.

It is noteworthy that the amount of Pd NPs influences greatly the sensing properties of SnO_2-ZnO C-S NWs. Functionalization (or decoration) with metal NPs has been used to further improve the sensing abilities of metal oxide NWs. Both electronic and chemical sensitizations are known to be responsible for the sensing improvement. A generally observed trend in the sensitivity of metal NPs-functionalized NWs corresponds to a bell-shaped curve as a function of the NP amount [39,40], indicating the need of optimizing the amount of functionalized Pd NPs.

Selective detection is one of the primary parameters that must be met prior to the actual implementation of the sensors. In that

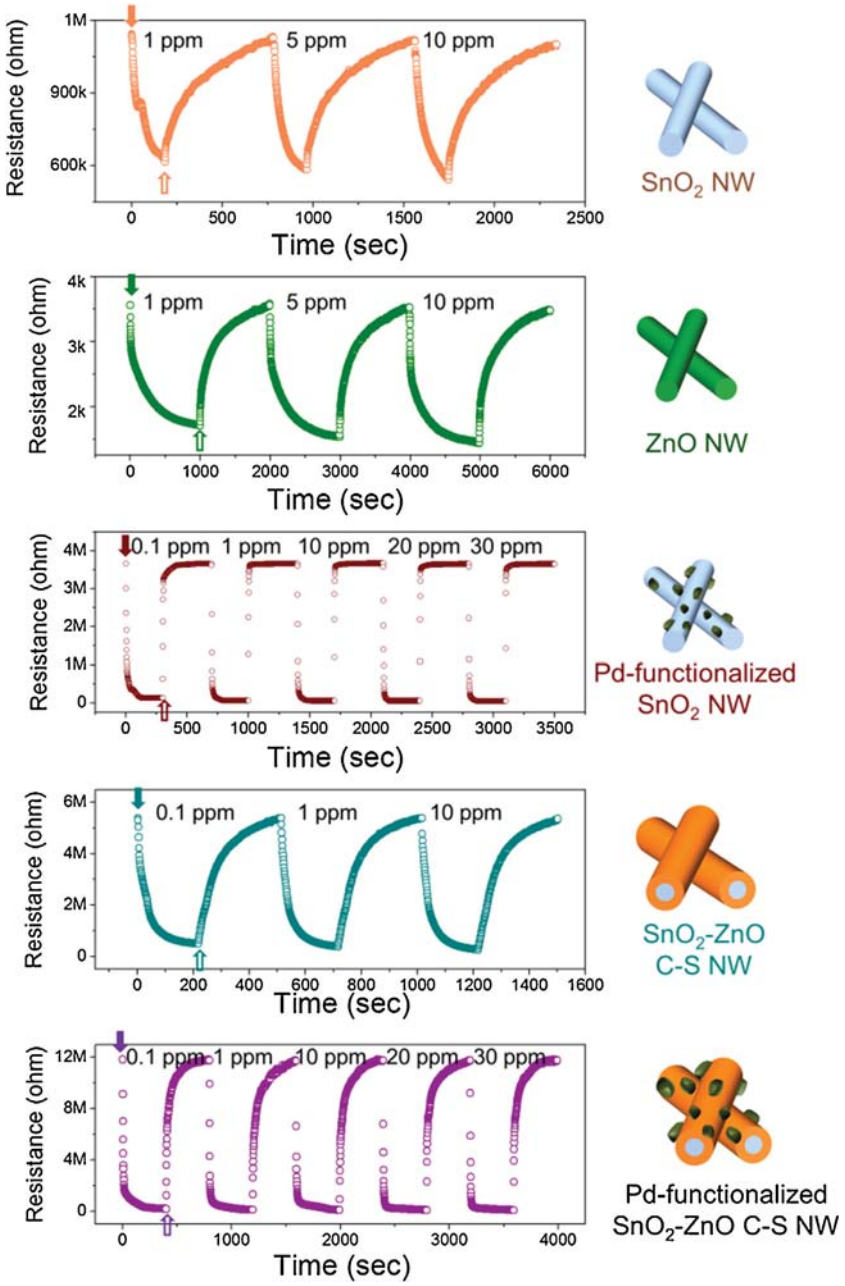

Fig. 2. Dynamic resistance curves of various NWs; pristine SnO_2 NWs, pristine ZnO NWs, Pd NPs-functionalized SnO_2 NWs, SnO_2-ZnO C-S NWs, and Pd NPs-functionalized SnO_2-ZnO C-S NWs for various C_6H_6 concentrations.

sense, the selectivity of the Pd NP-functionalized SnO_2-ZnO C-S NWs was evaluated by testing the sensing properties for other common reducing gases, such as CO, CO_2 and C_7H_8. Fig. 4a shows the dynamic resistance curves for the tested reducing gases at 100 ppb, and the corresponding sensor responses are summarized in Fig. 4b. The Pd NP-functionalized SnO_2-ZnO C-S NWs showed exceptional responses to C_6H_6, namely an approximately 8 times higher response compared to those of the other reducing gases. This shows that the approach based on the combination of SnO_2-ZnO C-S NWs and Pd NPs can provide a promising sensing platform for the selective detection of a trace amount of C_6H_6 gas.

The exceptionally high C_6H_6-sensing response realized in the SnO_2-ZnO C-S NWs functionalized with Pd NPs can be explained by the following mechanisms. First, the C-S NWs revealed superior sensing properties for reducing gases in the case of the optimized shell thickness compared to pristine core NWs [25]. In the hetero-junctions, the Fermi level of ZnO is supposed to be lower than that of SnO_2, with the work functions of ZnO and SnO_2 being about 5.2 and 4.9, respectively (Fig. 5a). The work function of bulk or films Pd can be set to 5.12 eV (Text S2 and Table S1 in Supplementary information). In our case, the work function of Pd nanoparticles will be smaller than 5.12 eV, because the work function of Pd nanoparticles is known to decrease with decreasing the diameter [41]. In order to equate to the Fermi level, electrons will be transferred not only from SnO_2 to ZnO, but also from Pd to ZnO. As a result of the charge transfer, a potential barrier will be generated at the heterointerfaces, along with the bending of the vacuum energy level and the energy band (Fig. 5a).

It is possible that the electrical current across the ZnO/SnO_2 heterointerfaces will provide an additional modulation of resistance (Fig. 5b). First, the sensor response can be explained by the variation of the potential barriers. The C_6H_6, which is a reducing gas,

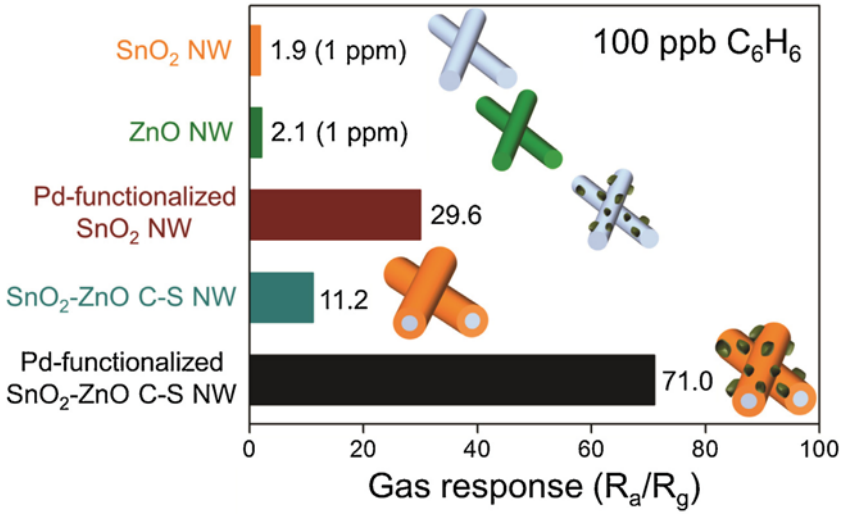

Fig. 3. Response of the Pd NPs-functionalized SnO_2-ZnO C-S NWs for 100 ppb of C_6H_6. For comparison purpose, the responses of the pristine SnO_2 NWs, pristine ZnO NWs, Pd NPs-functionalized SnO_2 NWs, and SnO_2-ZnO C-S NWs are included. Note that for the pristine SnO_2 NWs and pristine ZnO NWs, the responses for 1 ppm of C_6H_6 are included because they could not detect 100 ppb of C_6H_6.

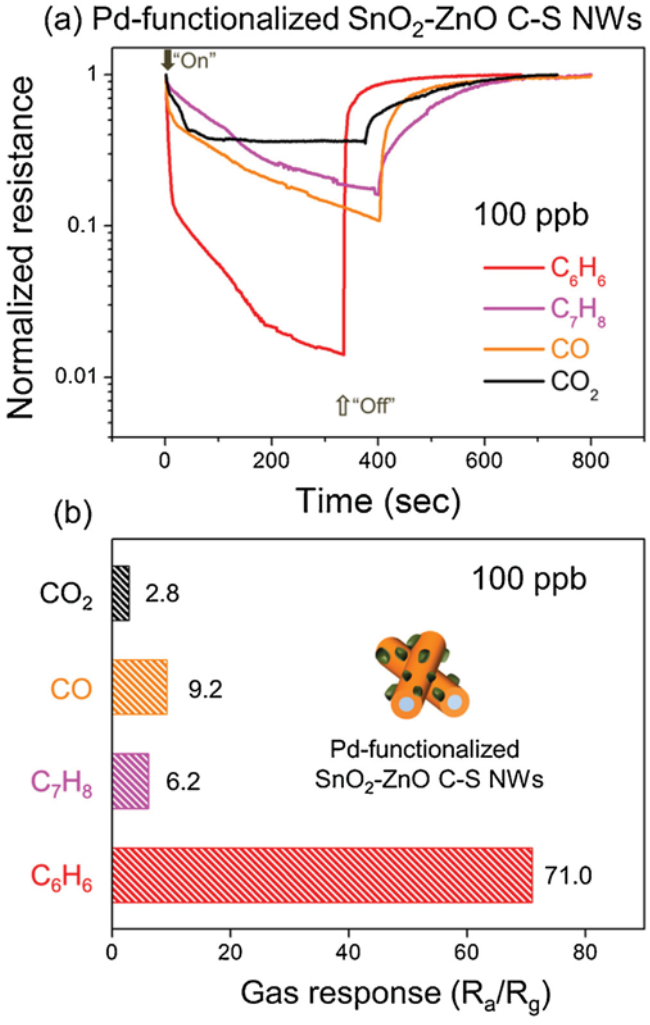

Fig. 4. (a) Dynamic resistance curves of the Pd NPs-functionalized SnO_2-ZnO C-S NWs for C_6H_6, C_7H_8, CO, and CO_2. (b) Summary of the responses for the gases tested.

will react with the adsorbed oxygen and release electrons by means of the following reaction: $C_6H_6 + 3O^-$ (ad) $\rightarrow N_2 + 3H_2O + 3e^-$ [42]. In this case, electrons will be transferred to the ZnO surface, elevating the Fermi level of ZnO. Accordingly, the reducing gas will decrease the height of the potential barriers (ZnO/SnO_2) to electrons. Therefore, the electrons in SnO_2 will more easily cross over to ZnO compared to the case in which the oxygen has been adsorbed. Since the introduction of C_6H_6 gas will decrease the resistance of ZnO, the reduction of the barrier layer will further decrease the resistance of ZnO, enhancing the sensitivity (i.e. R_g will be further reduced, increasing R_a/R_g, which is a definition of the sensor response). Second, the sensor response can be explained by the electron accumulation/depletion phenomenon. By the formation of a ZnO-SnO_2 heterojunction, the electron accumulation layer will be developed on the ZnO-side. However, upon the adsorption of oxygen ions, the electrons will be considerably drained form the ZnO surface, generating surface depletion regions (Fig. 5b). Furthermore, the introduction of the ZnO-SnO_2 heterointerface will increase the original conduction volume (or region) with a smaller initial resistance. Since the sensor response is defined as R_a/R_g, where R_a and R_g are the resistances in the absence and presence of the C_6H_6 gas, respectively, this mechanism will not contribute to the enhancement of the sensitivity; hence, this mechanism should be discarded. Accordingly, the generation of the ZnO-SnO_2 heterointerface is supposed to contribute to the sensor enhancement, in which the reducing gas will decrease the height of the potential barriers to electrons.

In addition, we expect that the functionalization with Pd NPs will introduce additional contributions to the sensing properties of the C-S NWs. One possibility will be related to the generation of a ZnO/Pd heterointerface (Fig. 6). Since electrons will flow from Pd to ZnO, electron accumulation will occur in the ZnO-side. The presence of Pd will decrease the initial resistance of ZnO. Accordingly, the donation of the same amount of the electrons by the introduction of C_6H_6 gas will slightly decrease the value of R_a/R_g, contributing to the decrease of the sensor response, discarding the mechanism in regard to the variation of ZnO/Pd heterointerface. The other contribution is chemical sensitization (CS) by the catalytic effect of the Pd NPs, shown in Fig. 5c, which facilitates more interactions between C_6H_6 and the adsorbed oxygen species, increasing the resistance modulation of the SnO_2-ZnO C-S NWs. According to previous reports [21,30], Pd was used to enhance the

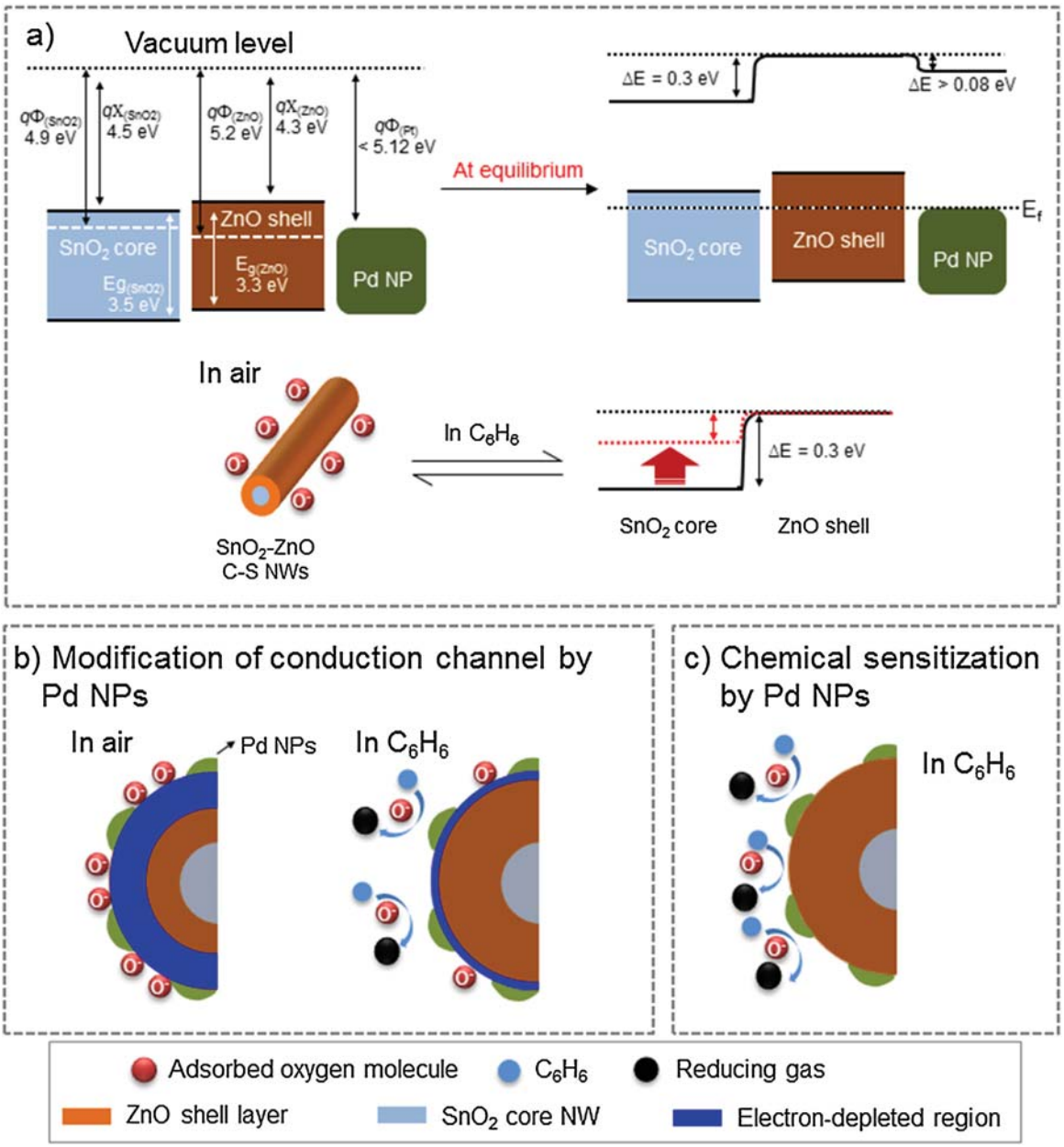

Fig. 5. Schematic diagrams illustrating the C_6H_6-sensing mechanisms of the Pd NPs-functionalized SnO_2-ZnO C-S NWs. (c) Energy-band diagrams resulting from the generation of heterojunctions. (b) Modification of the conduction channel in the shell layer and (c) the CS effect by the Pd NPs.

gas-sensing properties of semiconducting metal oxides. However, the precise reason why the Pd NPs are particularly effective with regards to C_6H_6 molecules has not been clarified yet. It is likely that the Pd NPs may dissociate the C_6H_6 gas more effectively than other reducing gases. Accordingly, with regard to ZnO-Pd heterointerfaces, chemical sensitization by the Pd NPs will play a role in enhancing the sensing behavior.

Table S2 in Supplementary information summarizes the response/recovery times of the various sensors studied in the present work. The C_6H_6 gas concentration was varied in the range of 0.1–30 ppm. For both SnO_2 and ZnO nanowires, we reveal that recovery times are longer than response times for all concentrations. By decorating with Pd nanoparticles, the response times of pristine SnO_2 nanowires were 93.7 and 93.3%-decreased, at 1 and 10 ppm, respectively. Also, the recovery times of pristine SnO_2 nanowires were 98.9 and 98.5%-decreased, at 1 and 10 ppm, respectively. By adding the ZnO shell with a thickness of 80 nm, the response times of pristine SnO_2 nanowires were 39.7 and 47.0%-decreased, at 1 and 10 ppm, respectively. Also, the recovery times of pristine SnO_2 nanowires were 61.9 and 56.9%-decreased, at 1 and 10 ppm, respectively. Furthermore, Pd-decoration obviously reduced the response/recovery times of the C-S NWs: By decorating with Pd nanoparticles, the response times of C-S NWs were 58.2, 80.3, and 80.3%-decreased, at 0.1, 1, and 10 ppm, respectively. Also, the recovery times of C-S NWs were 38.0, 3.5, and 12.6%-decreased, at 0.1, 1, and 10 ppm, respectively. Also, the recovery times of C-S NWs were 38.0, 3.5, and 12.6%-decreased, at 0.1, 1, and 10 ppm, respectively. For both pristine SnO_2 NWs and SnO_2-ZnO C-S NWs, Pd-functionalization decreased the recovery times as well as the response times. The catalytic effects of Pd will facilitate the adsorption of C_6H_6 gas molecules to Pd NPs. By the spillover effects, the adsorbed C_6H_6 gas molecules will be transferred to the neighboring SnO_2 (SnO_2 NWs) or ZnO surface (SnO_2-ZnO C-S NWs), providing more changes for sensing reactions. From Table S2, we

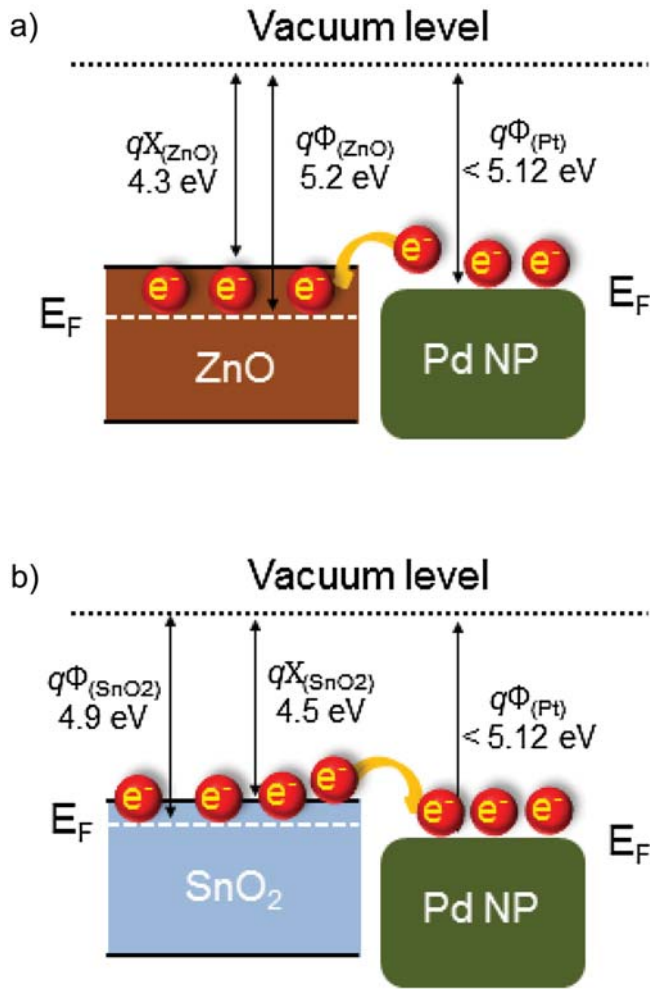

Fig. 6. Schematic diagrams illustrating the initial transfer of electrons upon the generation of heterostructures in (a) Pd NPs-functionalized SnO_2-ZnO C-S NWs and (b) SnO_2 pristine NWs.

reveal that both response times and recovery times were more significantly decreased by the Pd-functionalization, for pristine SnO_2 nanowires, in comparison to the SnO_2-ZnO C-S NWs. For pristine SnO_2 nanowires and SnO_2-ZnO C-S NWs, C_6H_6 gas molecules adsorb on SnO_2 and ZnO surfaces, respectively. For SnO_2-ZnO C-S NWs, by the Pd-functionalization, the ZnO/Pd heterojunction will be generated and the ZnO can become electron-accumulated by the electronic flow from Pd. This factor will not promote the adsorption of C_6H_6 gas molecules, which donate electrons to the ZnO surface. On the other hand, for SnO_2-ZnO C-S NWs, by the Pd-functionalization, the SnO_2/Pd heterojunction will be generated and the SnO_2 can become electron-depleted by the electronic flow towards Pd. This situation will favor the adsorption of C_6H_6 gas molecules, because the electron-deficient environment of SnO_2 will more likely capture the electrons. This will significantly reduce the response time. In addition, we surmise that the efficient adsorption will result in the abundant coverage of surface, bringing about the faster recovery process. For both pristine C-S NWs and Pd-functionalized SnO_2-ZnO C-S NWs, it is noteworthy that the recovery times are significantly longer than the response times. This observation will be related to the adsorption/desorption of the gas molecules. It is surmised that it takes longer time for gas species's desorption from the surface, than the adsorption to the surface.

4. Conclusions

In summary, with the hybrid structure of networked SnO_2-ZnO C-S NWs functionalized with Pd NPs, exceptionally high C_6H_6-sensing properties were achieved in a selective manner. The achieved response of 71 for 100 ppb is the highest C_6H_6 response reported thus far. The synergic effect via the additional expansion of the electron-depletion region in the shell layer and the catalytic role of the Pd NPs attached onto the shell surface is attributed to the selective, sensitive C_6H_6-sensing capability of the hybrid structure. The use of networked C-S NWs as a sensor platform and their functionalization with noble metal NPs was confirmed as a novel approach to the development of extremely sensitive, selective chemoresistive gas sensors potentially for the diagnosis of diseases. Also, Pd-functionalization decreased the recovery times as well as the response times. The generation of the ZnO-SnO_2 heterointerface will contribute to sensor enhancement, in which the reducing gas will decrease the height of the potential barriers of the electrons. In addition, the C-S will play a role in enhancing the sensing behavior because of the catalytic effect of the Pd NPs.

Acknowledgment

This research was supported by Basic Science Research Program through the National Research Foundation of Korea (NRF) funded by the Ministry of Education (2016R1A6A1A03013422).

Appendix A. Supplementary data

Supplementary data associated with this article can be found, in the online version, at http://dx.doi.org/10.1016/j.snb.2016.08.071.

References

[1] C. Ge, C. Xie, D. Zeng, S. Cai, Formaldehyde- benzene-, and xylene-sensing characterizations of Zn-W-O nanocomposite ceramics, J. Am. Ceram. Soc. 90 (2007) 3263–3267.
[2] M. Marbrook, P. Hawkins, Benzene sensing using thin films of titanium dioxide operating at room temperature, Sensors 2 (2002) 374–382.
[3] L. Wang, S. Wang, M. Xu, X. Hu, H. Zhang, Y. Wang, W. Huang, A Au-functionalized ZnO nanowire gas sensor for detection of benzene and toluene, Phys. Chem. Chem. Phys. 15 (2013) 17179–17186.
[4] I. Kheirbek, S. Johnson, Z. Ross, G. Pezeshki, K. Ito, H. Eisl, T. Matte, Spatial variability in levels of benzene, formaldehyde, and total benzene, toluene, ethylbenzene and xylenes in new york city: a land-use regression study, Environ. Health 11 (2012) 51.
[5] C.M. McHale, L. Zhang, M.T. Smith, Current understanding of the mechanism of benzene-induced leukemia in humans: implications for risk assessment, Carcinogenesis 33 (2012) 240–252.
[6] B. Sonawane, D. Bayliss, L. Valcovic, C. Chen, B. Rodan, W. Farland, Carcinogenic effects of benzene a status update and research needs to improve risk assessment: U. S. EPA perspective, J. Toxicol. Environ. Health A 61 (2000) 471–472.
[7] E. Song, J.-W. Choi, Conducting polyaniline nanowire and its applications in chemiresistive sensing, Nanomaterials 3 (2013) 498–523.
[8] S.M. Kanan, O.M. El-Kadri, I.A. Abu-Yousef, M.C. Kanan, Semiconducting metal oxide based sensors for selective gas pollutant detection, Sensors 9 (2009) 8158–8196.
[9] T. Zhang, S. Mubeen, N.V. Myung, M.A. Deshusses, Recent progress in carbon nanotube-based gas sensors, Nanotechnology 19 (2008) 332001.
[10] X. Du, S.M. George, Thickness dependence of sensor response for CO gas sensing by tin oxide films grown using atomic layer deposition, Sens. Actuators B 135 (2008) 152–160.
[11] S. Capone, A. Forleo, L. Francioso, R. Rella, P. Siciliano, J. Spadavecchia, D.S. Presicce, A.M. Taurino, Solid state gas sensors: state of the art and future activities, J. Optoelectron. Adv. Mater. 5 (2003) 1335–1348.
[12] U. Tisch, H. Haick, Nanomaterials for cross-reactive sensor arrays, MRS Bull. 35 (2010) 797–803.
[13] G.F. Fine, L.M. Cavanagh, A. Afonja, R. Binions, Metal oxide semi-conductor gas sensors in environmental monitoring, Sensors 10 (2010) 5469–5502.
[14] S. Zampolli, L. Elmi, J. Sturmann, S. Nicoletti, L. Dori, G.C. Cardinali, Selectivity enhancement of metal oxide gas sensors using a micromachined gas chromatographic column, Sens. Actuators B 105 (2005) 400–406.

[15] A.A. Tomchenko, G.P. Harmer, B.T. Marquis, Detection of chemical warfare agents using nanostructured metal oxide sensors, Sens. Actuators B 108 (2005) 41–55.
[16] I.-D. Kim, A.B. Rothschild, H. Lee, D.Y. Kim, S.M. Jo, H.L. Tuller, Ultrasensitive chemiresistors based on electrospun TiO_2 nanofibers, Nano Lett. 6 (2006) 2009–2013.
[17] J.B.K. Law, J.T.L. Thong, Improving the NH_3 gas sensitivity of ZnO nanowire sensors by reducing the carrier concentration, Nanotechnology 19 (2008) 205502.
[18] B. Wang, L.F. Zhu, Y.H. Yang, N.S. Xu, G.W. Yang, Fabrication of a SnO_2 nanowire gas sensor and sensor performance for hydrogen, J. Phys. Chem. C 112 (2008) 6643–6647.
[19] Q. Xiang, G. Meng, Y. Zhang, J. Xu, P. Xu, Q. Pan, W. Yu, Ag nanoparticle embedded-ZnO nanorods synthesized via a photochemical method and its gas-sensing properties, Sens. Actuators B 143 (2010) 635–640.
[20] V. Kumar, S. Sen, K.P. Muthe, N.K. Gaur, S.K. Gupta, J.V. Yakhmi, Copper doped SnO_2 nanowires as highly sensitive H_2S gas sensor, Sens. Actuators B 138 (2009) 587–590.
[21] A. Kolmakov, D.O. Klenov, Y. Lilach, S. Stemmer, M. Moskovits, Enhanced gas sensing by individual SnO_2 nanowires and nanobelts functionalized with Pd catalyst particles, Nano Lett. 5 (2005) 667–673.
[22] J.Y. Park, S.-W. Choi, S.S. Kim, Junction-tuned SnO_2 nanowires and their sensing properties, J. Phys. Chem. C 115 (2011) 12774–12781.
[23] J.-H. Kim, A. Katoch, S.-W. Choi, S.S. Kim, Growth and sensing properties of networked p-CuO nanowires, Sens. Actuators B 212 (2015) 190–195.
[24] J.Y. Park, Y.K. Park, S.S. Kim, Formation of networked ZnO nanowires by vapor phase growth and their sensing properties with respect to CO, Mater. Lett. 65 (2011) 2755–2757.
[25] S.-W. Choi, A. Katoch, G.-J. Sun, J.-H. Kim, S.-H. Kim, S.S. Kim, Dual functional sensing mechanism in SnO_2-ZnO core-shell nanowires, ACS Appl. Mater. Interfaces 6 (2014) 8281–8287.
[26] A. Katoch, J.-H. Kim, S.S. Kim, TiO_2/ZnO inner/outer double-layer hollow fibers for improved detection of reducing gases, ACS Appl. Mater. Interfaces 6 (2014) 21494–21499.
[27] J.Y. Park, S.-W. Choi, S.S. Kim, A synthesis and sensing application of hollow ZnO nanofibers with uniform wall thicknesses grown using polymer templates, Nanotechnology 21 (2010) 475601–475610.
[28] S.-W. Choi, J.Y. Park, C. Lee, J.G. Lee, S.S. Kim, Synthesis of highly crystalline hollow TiO_2 fibers using atomic layer deposition on polymer templates, J. Am. Ceram. Soc. 94 (2011) 1974–1977.
[29] J.Y. Park, S.-W. Choi, S.S. Kim, Tailoring the number of junctions per electrode pair in networked ZnO nanowire sensors, J. Am. Ceram. Soc. 94 (2011) 3922–3926.
[30] S.-W. Choi, S.-H. Jung, S.S. Kim, Functionalization of selectively grown networked SnO_2 nanowires with Pd nanodots by γ-ray radiolysis, Nanotechnology 22 (2011) 225501–225510.
[31] S.-W. Choi, J. Zhang, A. Katoch, S.S. Kim, H_2S sensing performance of electrospun CuO-loaded SnO_2 nanofibers, Sens. Actuators B 169 (2012) 54–60.
[32] S.-W. Choi, J. Zhang, A. Katoch, S.S. Kim, Significant enhancement of the sensing characteristics of In_2O_3 nanowires by functionalization with Pt nanoparticles, Nanotechnology 21 (2010) 415502–415509.
[33] J. Huang, L. Wang, C. Gu, Z. Wang, Y. Sun, J.-J. Shim, Preparation of porous SnO_2 microcubes and their enhanced gas-sensing property, Sens. Actuators B 207 (2015) 782–790.
[34] C. Song, C. Li, Y. Yin, J. Xiao, X. Zhang, M. Song, W. Dong, Preparation and gas sensing properties of partially broken WO_3 nanotubes, Vacuum (2015) 13–16.
[35] Y.J. Hong, J.-W. Yoon, J.-H. Lee, Yun Chan Kang, One-pot synthesis of Pd-loaded SnO_2 yolk-shell nanostructures for ultraselective methyl benzene sensors, Chem. Eur. J. 20 (2014) 2737–2741.
[36] L. Wang, S. Wang, H. Zhang, Y. Wang, J. Yang, W. Huang, Au-functionalized porous ZnO microsheets and their enhanced gas sensing properties, New J. Chem. 38 (2014) 2530–2537.
[37] C. Ge, C. Xie, S. Cai, Preparation and gas-sensing properties of Ce-doped ZnO thin-film sensors by dip-coating, Mater. Sci. Eng. B 137 (2007) 53–58.
[38] M. Mabrook, P.A. Hawkins, Rapidly-responding sensor for benzene, methanol and ethanol vapours based on films of titanium dioxide dispersed in a polymer operating at room temperature, Sens. Actuators B 75 (2001) 197–202.
[39] J. Ding, J.W. Zhu, P.C. Yao, J. Li, H.P. Bi, X. Wang, Synthesis of ZnO-Ag hybrids and their gas-sensing performance toward ethanol, Ind. Eng. Chem. Res. 54 (2015) 8947–8953.
[40] I.S. Hwang, J.K. Choi, H.S. Woo, S.J. Kim, S.Y. Jung, T.Y. Seong, et al., Facile control of C_2H_5OH sensing characteristics by decorating discrete Ag nanoclusters on SnO_2 nanowire networks, ACS Appl. Mater. Interfaces 3 (2011) 3140–3145.
[41] A. Kumar, D.A. Buttry, Size-dependent underpotential deposition of copper on palladium nanoparticles, J. Phys. Chem. C 119 (2015) 16927–16933.
[42] B.T. Marquis, J.F. Vetelino, A semiconducting metal oxide sensor array for the detection of NO_x and NH_3, Sens. Actuators B 77 (2001) 100–110.

Biographies

Jae-Hun Kim received his B.S. degree from Gyeongsang National University, Republic of Korea in 2013. In February 2015, he received M.S. degree from Inha University, Republic of Korea. He is now working as a Ph. D. candidate at Inha University, Republic of Korea. He has been working on oxide nanowire gas sensors.

Hyoun Woo Kim joined the Division of Materials Science and Engineering at Hanyang University as a full professor in 2011. He received his B.S. and M. S. degrees from Seoul National University and his Ph.D. degree from Massachusetts Institute of Technology (MIT) in electronic materials in 1986, 1988, and 1994, respectively. He was a senior researcher in the Samsung Electronics Co., Ltd. from 1994 to 2000. He has been a professor of materials science and engineering at Inha University from 2000 to 2010. He was a visiting professor at the Department of Chemistry of the Michigan State University, in 2009. His research interests include the one-dimensional nanostructures, nanosheets, and gas sensors.

Sang Sub Kim joined the School of Materials Science and Engineering, Inha University, in 2007 as a full professor. He received his B.S. degree from Seoul National University and his M.S and Ph.D. degrees from Pohang University of Science and Technology (POSTECH) in Material Science and Engineering in 1987, 1990, and 1994, respectively. He was a visiting researcher at National Research in Inorganic Materials (currently NIMS), Japan for 2 years each in 1995 and in 2000. In 2006, he was a visiting professor at Department of Chemistry, University of Alberta, Canada. In 2010, he also served as a cooperative professor at Nagaoka University of Technology, Japan. His research interests include the synthesis and applications of nanomaterials such as nanowires and nanofibers, functional thin films, and surface and interfacial characterizations.

Supplementary Information

Ultra-sensitive benzene detection by a novel approach: core-shell nanowires combined with the Pd-functionalization

Jae-Hun Kim[a], Hyoun Woo Kim[b,c*] and Sang Sub Kim[a*]

[a]Department of Materials Science and Engineering, Inha University, Incheon 402-751, Republic of Korea

[b]Division of Materials Science and Engineering, Hanyang University, Seoul 133-791, Republic of Korea

[c]The Research Institute of Industrial Science, Hanyang University, Seoul 133-791, Republic of Korea

[a)] Corresponding author.
E-mail address:sangsub@inha.ac.kr (S.S. Kim). hyounwoo@hanyang.ac.kr (H.W. Kim)

Text S1.

In our previous work, we prepared the networked SnO_2 nanowires and carried out the sensing tests in regard to NO_2 gas [1]. The sensitivity for the sensor has been investigated as a function of temperature under various NO_2 concentrations and the results are summarized in Figure 7b of Ref. 1. At a given NO_2 concentration, the sensor response increases as the temperature increases until 300°C, and then it tends to decrease with further temperature increase until 400℃. The temperature showing the best sensitivity (sensor response) for each concentration is around 300℃. At the NO_2 concentration of 70 ppm, however, the temperature showing the best sensitivity (sensor response) is around 350℃. The same processing parameters were used for growth of SnO_2 nanowires in the present work, indicating that the optimum operating temperature of the SnO_2 nanowires can be considered to be around 300℃. In our previous work, we prepared the networked ZnO nanowires and carried out the sensing tests in regard to NO_2 gas [2]. Sensing properties of the networked nanowire sensors to NO_2 were investigated. The sensor response was measured as a function of temperature under various NO_2 concentration, and the results are summarized in Figure 4(a) of Ref. 2. The concentration was varied in the range of 1-70 ppm. At NO_2 concentration of 1-10 ppm and 60-70 ppm, the sensor response increases as the temperature increases until 350℃, and then it tends to decrease with further temperature increase until 400℃. The temperature showing the best sensitivity for each concentration is around 350℃. On the other hand, at NO_2 concentration of 20-50 ppm, the sensor response increases as the

temperature increases until 300℃, and then it tends to decrease with further temperature increase until 400℃. The temperature showing the best sensitivity for each concentration is around 300℃. To summarize, at NO_2 concentration of 1-70 ppm, the temperature showing the best sensitivity for each concentration is around 300-350℃. Therefore, it is reasonable to compare the sensing responses of ZnO nanowires to other types of nanowires sensors including SnO_2 nanowires, core-shell nanowires, and etc. In addition, according to our other investigations [3], in which SnO_2 nanowires, synthesized by using the same conditions as the ones in the present work, were decorated with metal nanoparticles such as Pt, Pd, and Au. Their sensing performances were investigated for various gases (C_6H_6, C_7H_8, CO, C_2H_5OH, and H_2S), and the optimum operating temperature of the fabricated sensors was around 300 °C. Also, by the examination of the thermodynamics of the Pd-decorated SnO_2 nanowires system (i.e. commercial software package, FactSage), we reveal that there is no obvious change in the gas phase chemistry in the tested temperature range of 35-400°C. It implies that the Pd-functionalization does not significantly change the gas-phase chemistry at temperature in the range of 35-400°C. Although the optimum operating temperature may be slightly different with regards to the kind of gases for other sensing materials and systems, all of the sensors in the present work showed it around 300°C. With the preliminary information on the sensing behaviour of SnO_2 and ZnO networked nanowires as a functional of the operating temperature, we carried out the sensing tests, to reveal the effect of temperature on the sensing behaviour of Pd NPs-functionalized SnO_2-ZnO C-S NWs (Fig. S2). The C_6H_6 concentration was set to 0.1 ppm and the

temperature was varied in the range of 200-400℃. At C_6H_6 concentration of 0.1 ppm, the sensor response increases as the temperature increases until 300℃, and then it tends to decrease with further temperature increase until 400℃. The temperature showing the best sensitivity for each concentration is around 300℃. From our previous works and complementary experiments, it is reasonable to compare the sensing properties of a variety of materials, including SnO_2 NWs, ZnO MWs, Pd-functionalized SnO_2 NWs, C-S NW, and Pd-functionalized C-S NWs at the same temperature of 300°C (Fig. 3 in the main text).

Text S2.

Actually, many literatures reported the values of the work function of Pd. In Table S1, we summarize the work function values of Pd [4-15]. The work function value is known to depend on a variety of factors, including surface condition and morphology. An exceptionally high value of 5.83 eV was reported for Pd (110), which had been measured by ultraviolet photoemission spectroscopy (UPS). The UPS spectra were obtained from oxygen-covered Pd(110). However, most calculated or measured work functions of Pd are smaller than 5.2 eV. By the way, many literatures have cited the value of 5.12 eV, which is originated from the Sze's book [13]. In addition, the work function of Pd nanoparticles is known to decrease with decreasing the diameter in the range of 4.8-5.0 eV [11]. Similarly, the work function of Au nanoparticles is size-dependent, being significantly smaller than that of bulk Au [16]. Since the average diameter of Pd nanoparticles in the present work is about 15 nm, it is probable that the actual work function will be smaller than 5.12 eV.

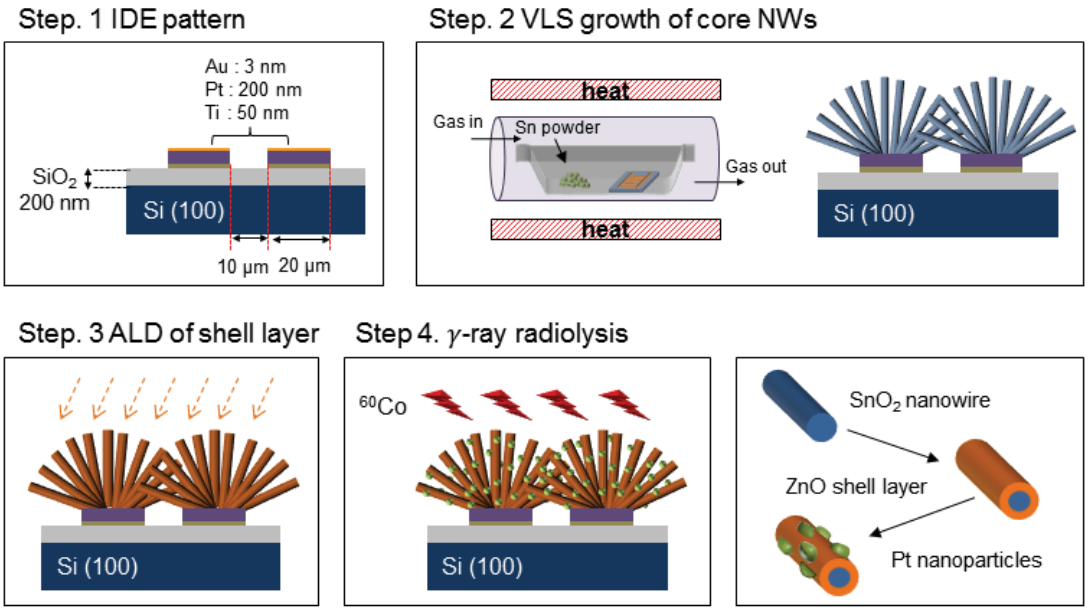

Figure S1. Schematic illustration of the fabrication for Pd Nanoparticle-functionalized core-shell nanowires.

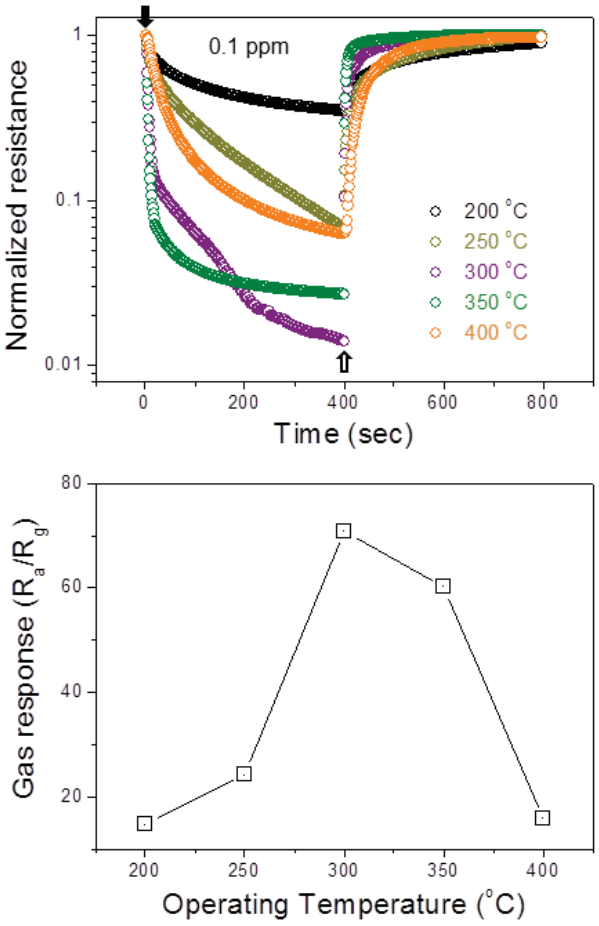

Figure S2. Variation of normailzed resistance and sensor responses of Pd Nanoparticle-functionalized core-shell nanowires with varying the operating temperature in the range of 200-400°C. The C_6H_6 concentration was set to 0.1 ppm.

Table S1. Summary of the work function values of Pd, which were reported in the previous literatures.

Material type	Value of work function (eV)	Reference
Pd plate	4.99	[4]
Pd nanoparticle	5.0	[5]
Pd thin films (vacuum)	5.12	[6]
Pd thin films (measured)	4.79	[6]
Bulk Pd	5.12	[7]
Slab-Pd (111) (cal.)	5.25	[8]
Slab-Pd (100) (cal.)	5.11	[8]
Slab-Pd (110) (cal.)	4.87	[8]
Bulk-Pd (110)	5.83	[9]
Pd thin film (273K) (vacuum)	5.11	[10]
Pd thin film (573K) (vacuum)	5.22	[10]
Pd NPs (average diameter 98±38 nm)	5.0	[11]
Pd NPs (average diameter 3.1±0.7 nm)	4.88	[11]
Pd NPs (average diameter 2.4±0.5 nm)	4.85	[11]
Pd NPs (average diameter 1.6±0.4 nm)	4.77	[11]
Pd thin films	5.12	[12],[13]
Metallic Pd	4.8	[14],[15]

Table S2. Summary of the response/recovery times of the various sensors studied in the present work. The C_6H_6 gas concentration was varied in the range of 0.1-30 ppm.

Material type	Response time (s)						Recovery time (s)					
	0.1	**1**	**5**	**10**	**20**	**30**	**0.1**	**1**	**5**	**10**	**20**	**30**
SnO2 NWs	-	126	101	134	-	-	-	449	415	406	-	-
ZnO NWs	-	499	461	406	-	-	-	654	617	588	-	-
Pd-functionalized SnO_2 NWs	27	8	-	9	8	6	13	5	-	6	5	5
SnO_2-ZnO C-S NWs (shell thickness 80 nm)	79	76	-	71	-	-	184	171	-	175	-	-
Pd-functionalized SnO_2-ZnO C-S NWs (shell thickness 80 nm)	33	15	-	14	10	9	114	165	-	153	147	128

References

[1] J. Y. Kim, S.-W. Choi, S. S. Kim, Junction-tuned SnO_2 nanowires and their sensing properties. J. Phys. Chem. C 115 (2011) 12774-12781.

[2] J. Y. Kim, S.-W. Choi, S. S. Kim, Tailoring the number of junctions per electrode pair in networked ZnO nanowire sensors. J. Am. Ceram. Soc. 94 (2011) 3922-3926.

[3] J.-H. Kim, P. Wu, H. W. Kim, S. S. Kim, Highly selective sensing of CO, C_6H_6, and C_7H_8 gases by catalytic functionalization with metal nanoparticles, ACS Appl. Mater. Interfaces 8 (2016) 7173-7183.

[4] D. Yamashita, A. Ishizaki, In situ measurements of change in work function of Pt, Pd and Au surfaces during desorption of oxygen by using photoemission yield spectrometer in air, Appl. Surf. Sci. 363 (2016) 240-244.

[5] J.-H. Ahn, J. Yun, Y.-K. Choi, I. Park, Palladium nanoparticle decorated silicon nanowire field-effect transistor with side-gates for hydrogen detection, Appl. Phys. Lett. 104 (2014) 013508.

[6] D. Gu, S. K. Dey, P. Majhi, Effective work function of Pt, Pd, and Re on atomic layer deposited HfO_2, Appl. Phys. Lett. 89 (2006) 082907.

[7] H. B. Michaelson, The work function of the elements and its periodicity, J. Appl. Phys. 48 (1977) 4729-4733.

[8] N. E. Singh-Miller, N. Marzari, Surface energies, work functions, and surface

relaxations of low-index metallic surfaces from first principles, Phy. Rev. B 80 (2009) 235407.

[9] V. A. Bondzie, P. Kleban, D. J. Dwyer, XPS identification of the chemical state of subsurface oxygen in the O/Pd(110) system, Surf. Sci. 347 (1996) 319-328.

[10] R. Bouwman, G. J. M. Lippits, W. M. H. Sachtler, Photoelectric investigation of the surface composition of equilibrated Ag-Pd alloys in ultrahigh vacuum and in the presence of CO, J. Catal. 25 (1972) 350-361.

[11] A. Kumar, D. A. Buttry, Size-dependent underpotential deposition of copper on palladium nanoparticles, J. Phys. Chem. C 119 (2015) 16927-16933.

[12] Y. M. Wong, W. P. Kang, J. L. Davidson, A. Wisitsora-at, K. L. Soh, A novel microelectronic gas sensor utilizing carbon nanotubes for hydrogen gas detection, Sens. Actuators, B 93 (2003) 327-332.

[13] S. M. Sze, Physics of Semiconductor Devices, Wiley, New York, 1981.

[14] E. Czerwosz, D. Vouagner, P. Dluzawski, K. Zawada, J. P. Girardeau-Montaut, Vacuum 63 (2001) 355-360.

[15] V. S. Fomenko, Handbook of thermoionic properties, New York, 1966.

[16] Y. Zhang, O. Pluchery, L. Caillard, A.-F. Lamic-Humblot, S. Casale, Y. J. Chabal, M. Salmeron, Sensing the charge state of single gold nanoparticles vis work function measurements, Nano Lett. 15 (2015) 51-55.